Exploring DMS oxidation and implications for global aerosol radiative forcing

Ka Ming Fung[1], Colette L. Heald[1,2], Jesse H. Kroll[1], Siyuan Wang[3], Duseong S. Jo[4], Andrew Gettelman[4], Zheng Lu[5], Xiaohong Liu[5], Rahul A. Zaveri[6], Eric Apel[4], Donald R. Blake[7], Jose-Luis Jimenez[8], Pedro Campuzano-Jost[8], Patrick Veres[3], Timothy S. Bates[9], John E. Shilling[10], Maria Zawadowicz[11]

[1] Department of Civil and Environmental Engineering, Massachusetts Institute of Technology, Cambridge, MA, USA

[2] Department of Earth, Atmospheric and Planetary Sciences, Massachusetts Institute of Technology, Cambridge, MA, USA

[3] Chemical Sciences Laboratory, National Oceanic and Atmospheric Administration, Boulder, CO, USA

[4] Atmospheric Chemistry Observations and Modeling Laboratory, National Center for Atmospheric Research, Boulder, CO, USA

[5] Department of Atmospheric Sciences, Texas A&M University, College Station, TX, USA

[6] Pacific Northwest National Laboratory, Richland, WA, USA

[7] Department of Chemistry, University of California, Irvine, CA, USA

[8] Department of Chemistry & Cooperative Institute for Research in Environmental Sciences, University of Colorado, Boulder, CO, USA

[9] The Cooperative Institute for Climate, Ocean, and Ecosystem Studies, College of the Environment, University of Washington, Seattle, WA, USA

[10] Atmospheric Sciences and Global Change Division, Pacific Northwest National Laboratory, Richland, WA, USA

[11] Environmental and Climate Sciences Department, Brookhaven National Laboratory, Upton, NY, USA

Corresponding to: Ka Ming Fung (kamingfung@mit.edu) & Colette L. Heald (heald@mit.edu)

Supplementary Information

1 Detailed model description

1.1 Cloud-borne Aerosols

In-cloud aqueous-phase reactions are handled separately in CAM6-chem (Barth et al., 2000; Rasch et al., 2000). After the chemical production and loss in the gas-phase reactions and the aqueous-phase within the interstitial aerosols, the amounts of SO_2, MSA, and H_2SO_4 collected by cloud are computed based on their concentrations, effective Henry's Law constants, and cloud fraction in each grid cell. For each cloudy grid cell, the gas-aqueous equilibrium is controlled by the equilibrium pH of local bulk cloud water. Such equilibrium pH is evaluated by iteratively solving an electro-neutrality equation that balances the charges of all dissolved species, including H^+, NH_4^+, Na^+, Ca^{2+}, OH^-, Cl^-, NO_3^-, HCO_3^-, HSO_3^-, SO_3^{2-}, and SO_4^{2-}. Based on this equilibrium pH, a portion of available SO_2 is dissolved in cloud water and oxidized by H_2O_2 and O_3, forming cloud-borne sulfate aerosol. Another source of cloud-borne sulfate is cloud uptake of MSA and H_2SO_4. Gains in sulfate mass from these in-cloud processes are contributed to each mode in proportion to its relative aerosol number abundance, and it is assumed that no new particles are formed.

1.2 Aerosol Formation and Growth

Aerosol formation and growth in CAM6-chem are treated by MAM4 (Liu et al., 2016), we do not modify these schemes in our work, but provide a short description of relevant processes here.

New particle formation initiated by clusters of H_2SO_4 vapor is modeled through three regime-based parameterizations (He and Zhang, 2014), namely, 1) H_2SO_4-NH_3-H_2O ternary nucleation when NH_3 > 0.1 ppt (Merikanto et al., 2007); 2) H_2SO_4-H_2O binary nucleation when NH_3 is low or absent (Vehkamäki, 2002), and; 3) empirical formulas depending solely on the concentration of H_2SO_4 to

reduce the model low-bias of boundary layer nucleation rate (Wang and Penner, 2009). All nucleation processes are assumed to occur in the vapor phase homogeneously. Loss due to coagulation as new particles grow from critical clusters to Aitken mode is accounted for following the treatment in Kerminen and Kulmala (2002). The remaining new particles are added to both number and mass of Aitken mode sulfate and ammonium aerosols.

Condensation of H_2SO_4 and NH_3 vapors on aerosol particles follows Zaveri et al. (2008). Aerosol uptake of NH_3 ceases when the local mass ratio of NH_4^+/SO_4^{2-} reaches two. This dynamic process contributes to aerosol size growth. Aerosols in Aitken and accumulation modes that grow larger than the model-defined size-bin boundary will trigger reassignment of number and mass from their original modes to accumulation and coarse modes correspondingly.

Coagulation rates of Aitken and accumulation aerosols are calculated using the fast/approximate algorithms of community Multiscale Air Quality (CMAQ) model 4.6 while the much slower coagulation processes involving the coarse mode aerosol are neglected (Binkowski and Roselle, 2003). Intramodal coagulation results in a reduction in particle number in corresponding modes but their totals remain unchanged. Intermodal coagulation reduces the number of Aitken mode aerosols and transfers masses from the Aitken mode to the accumulation mode.

Water uptake by aerosol is handled by MOSAIC (Zaveri et al., 2008, 2021). The bulk hygroscopicity of each mode is determined as the volume-weighted mean hygroscopicity of all components in that mode. Values of the hygroscopicity for sulfate (0.507) and other aerosols are from Petters and Kreidenweis (2007) and various references detailed in Liu et al. (2012). Due to its high hygroscopicity, higher sulfate concentration results in enhanced water uptake capability of airborne aerosols.

Interstitial aerosols are activated and become cloud-borne under sub-grid vertical mixing with the presence of cloud. The activation is parameterized as a function of updraft velocity and the averaged properties of all aerosol modes (Abdul-Razzak and Ghan, 2000). During activation, the model transfers

both mass and number of aerosols from the interstitial attachment state to the cloud-borne state. This process can trigger new cloud formation or increase the aerosol loading of existing cloud. CAM6-chem assumes a three-hour in-cloud residence time for air parcels (Lelieveld and Crutzen, 1990), i.e., 1/6 of the cloud-borne aerosol is dissipated and re-suspended as air-borne particles after each model timestep of 30 minutes.

1.3 Dry & Wet Deposition

Gravity- and turbulence-driven dry deposition processes are considered in CAM6-chem. All species above the surface layer are subject to gravitational settling at velocities determined following Seinfeld et al., (1998). Turbulent dry deposition is handled based on the resistance approach with phase-dependent adjustments (Emmons et al., 2010; Wesely, 1989). For gas-phase species, the model calculates the aerodynamic and the boundary resistances based on online atmosphere dynamics, while the surface resistance over land is determined according to online CLM5 surface variables, e.g., canopy height and leaf area index (LAI), as well as species-dependent reactivity factor for oxidation and effective Henry's Law constants. For aerosols, the aerodynamic resistance is the same as that of gases, but the boundary and surface resistances are replaced by a single resistance term which depends on the surface friction velocity. Deposition velocities are evaluated as the reciprocal of the sum of their corresponding resistance terms, and deposition rates are the product of their deposition velocities and concentrations.

Wet deposition of gaseous chemicals in CAM6-chem is handled by the Neu and Prather (2012) scheme which assumes a first-order loss due to in-cloud and below-cloud scavenging processes. The wet removal rate of a depositing gas is the product of its concentration, loss frequency (depending on its effective Henry's Law coefficients), and the fraction of the grid box that is undergoing scavenging events, such as the presence of cloud or precipitation. Aerosol wet removal is handled using a separate routine (Barth et al., 2000; Liu et al., 2012). In-cloud aerosol removal rates depend on the mass mixing

ratio of activated aerosols and precipitation rates. Below-cloud scavenging of interstitial aerosols is assumed a first-order removal process and the removal rate is determined by the product of scavenging coefficient and precipitation rate.

1.4 Cloud

CAM6-chem simulates the fate of cloud liquid drops/ice crystals using the two-moment microphysics (MG2) for prognostic evolution of mass and number mixing ratios of cloud (Gettelman and Morrison, 2015). This scheme is coupled to MAM4 for droplet activation (Abdul-Razzak and Ghan, 2000) and ice nucleation (Liu et al., 2007). Briefly, the fraction of activation is controlled by critical superstation of particles, which depends on, e.g., bulk hygroscopicity and size distribution of aerosols. Occurrence of stratiform, shallow convective, and deep convective cloud are predicted by the Cloud Layers Unified by Binormals (CLUBB) scheme (Bogenschutz et al., 2012, 2018; Golaz and Larson, 2002). This scheme also enables the simulation of prognostic precipitation, including the autoconversion of CCN and accretion by rain or snow (Gettelman, 2015; Gettelman and Morrison, 2015).

1.5 Radiative Transfer

Longwave (LW) and shortwave (SW) radiative transfer within CAM6-Chem are represented by the broadband k-distribution Rapid Radiative Transfer Model for Global Circulation Models (RRTMG) (Iacono et al., 2008) with sixteen LW and fourteen SW spectral intervals. RRTMG is coupled with the aerosol and cloud schemes in CAM6-chem for spatial distribution and optical properties of the condensed-phase particles, drops, and ice crystals. Absorption by aerosols and clouds is included for LW while extinction by aerosols and cloud drops is considered for SW. Mass-specific aerosol optical properties are parameterized as functions of wet refractive index and mode wet surface radius for each

band of SW (extinction, single-scattering albedo, and asymmetry parameter) and LW (mass-specific absorption) (Ghan and Zaveri, 2007). Sulfate refractive indices at visible wavelengths are $1.43 + 0.00i$ (Hess et al., 1998). Liquid cloud optics is parameterized following the gamma size distribution implemented by Morrison and Gettelman (2008). Ice cloud optics is also determined using a similar look-up approach produced by the modified anomalous diffraction approximation (MADA) (Mitchell et al., 2006). Sub-grid variabilities of cloudiness and cloud overlapping are handled using the Monte-Carlo Independent Column Approximation (McICA) (Pincus et al., 2003).

1.6 Radiative Forcing

We follow Ghan (2013) to quantify sulfate direct radiative effect (DRE) as ($F - F_{\text{sulfate-free}}$), where F is the SW radiative flux at the top of the atmosphere (TOA), and $F_{\text{sulfate-free}}$ the flux computed by CAM6-chem as a diagnostic by neglecting sulfate. Sulfate direct radiative forcing (DRF) is determined by differencing the DRE of a pair of simulations with the PD and PI emissions. Finally, we estimate sulfate indirect radiative forcing (IRF) as the change in cloud radiative effect (CRE), which equals to ($F - F_{\text{clear}}$), where F_{clear} is the flux computed by the model with cloud neglected, between a pair of simulations with different atmospheric conditions.

2 Present-day spatial distribution of atmospheric sulfur and oxidants involved in our DMS oxidation scheme

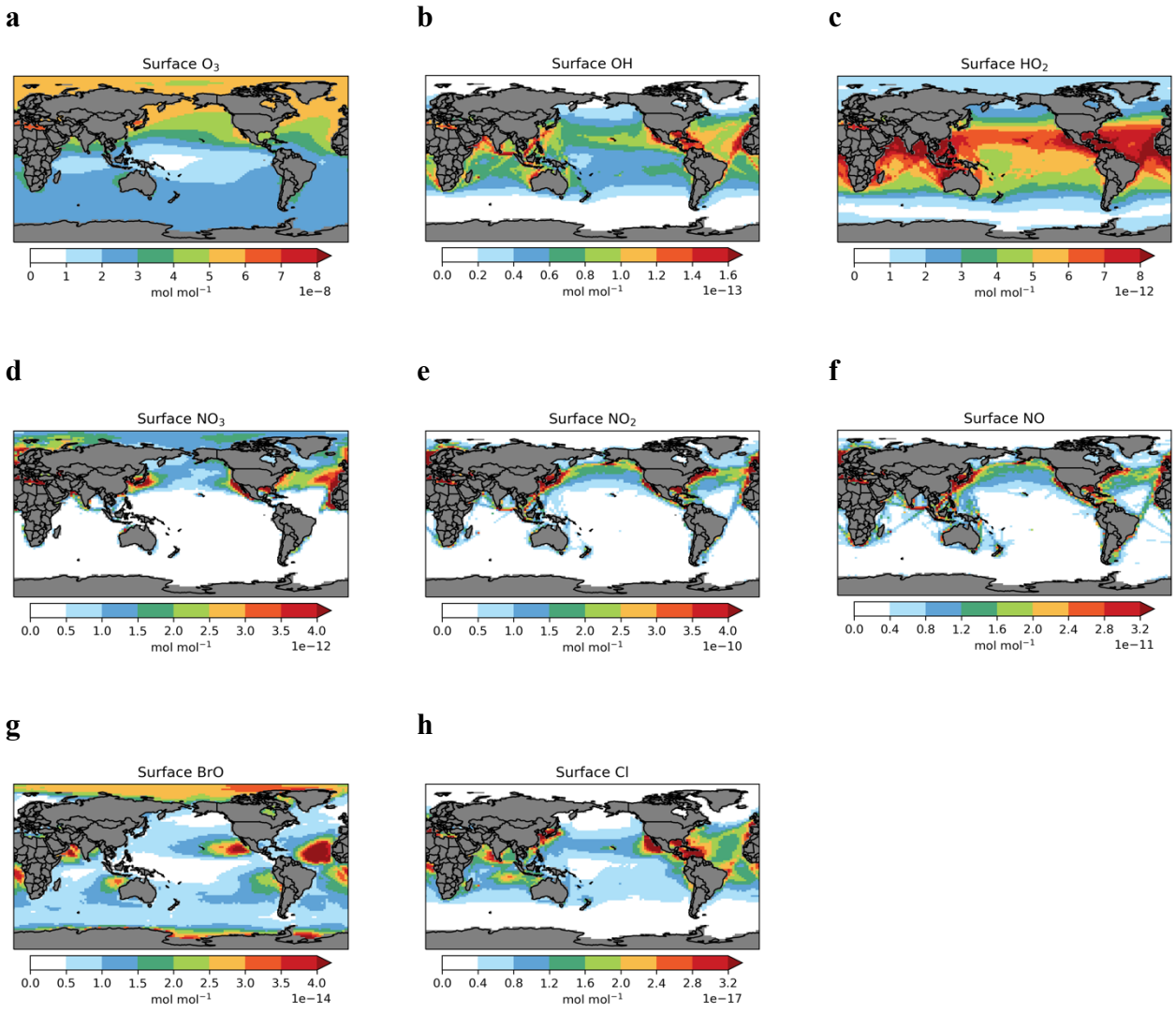

Figure S1. Annual-mean surface concentrations of major oxidants involving in our modified DMS chemistry.

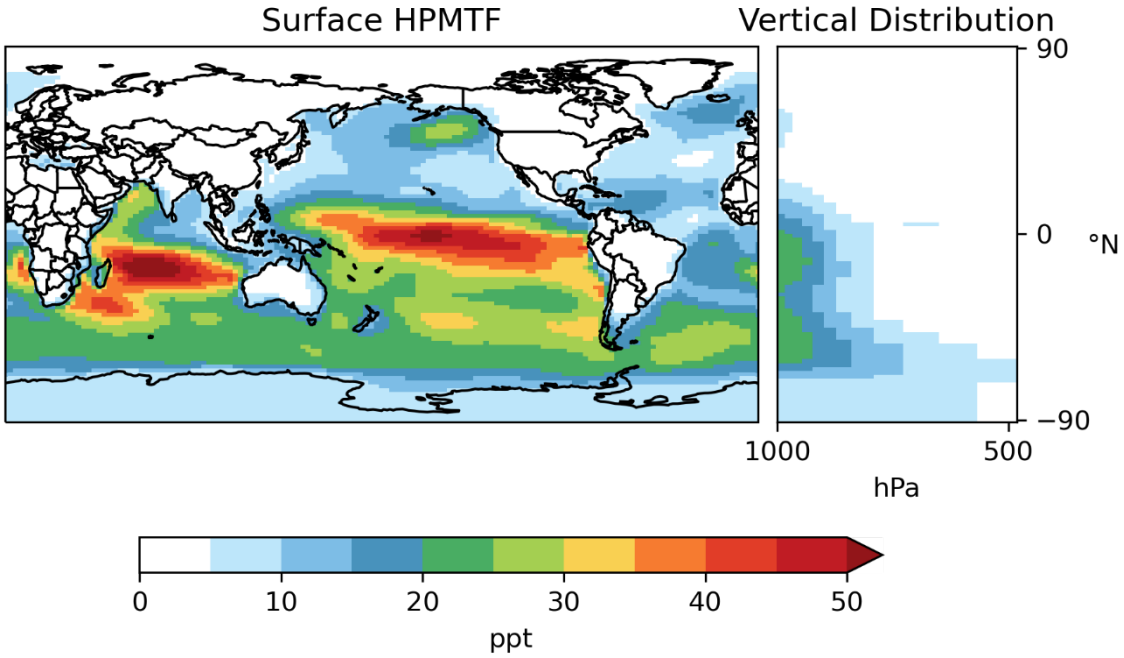

Figure S2. Horizontal distribution of annual-mean surface mixing ratio and zonal-mean vertical distribution for HPMTF.

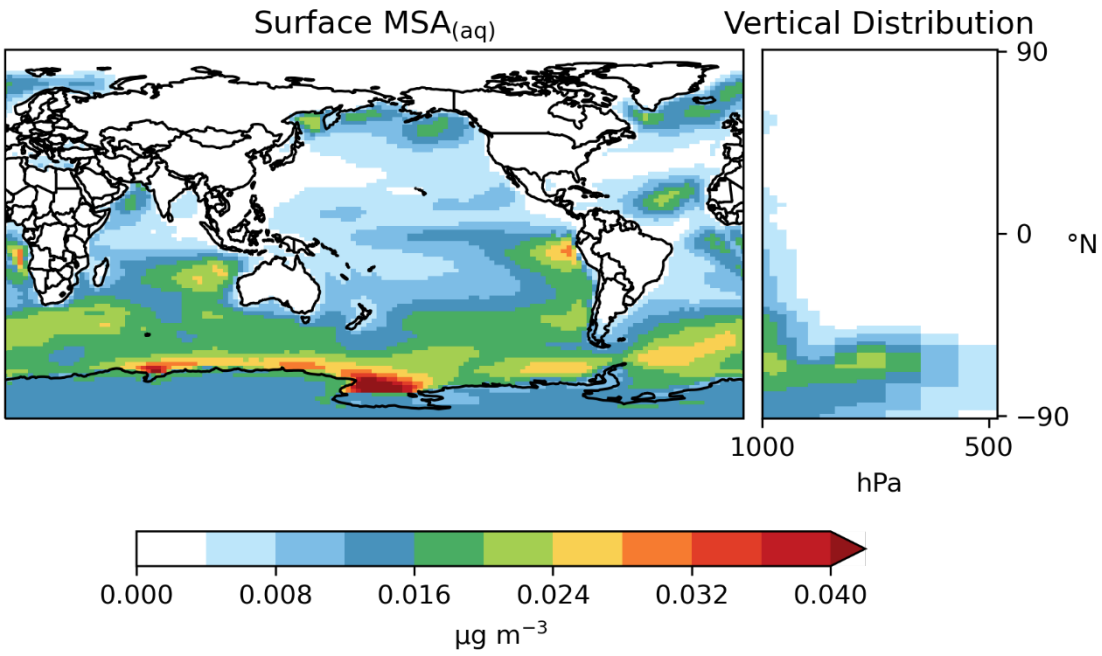

Figure S3. Horizontal distribution of annual-mean surface concentration and zonal-mean vertical distribution for MSA aerosol.

150

3 Uncertainty in DMS emission

We employed the OASISS flux scheme and calculated the DMS ocean-to-air fluxes based on sea-surface DMS concentration climatology generated by Lana et al. (2011). Their climatology map was based on a series of site measurements and extrapolation of the data for months when data is
155 unavailable. Data are scarce in remote regions such as the Southern Ocean, resulting in larger uncertainty in surface DMS concentration. Such uncertainty propagates to our DMS flux estimates, particularly over the Southern. We hence performed a sensitivity test on [MOD_2000] by reducing the sea surface DMS concentration in regions south to 30ºS by 50% (aliased as [MOD_lessSDMS_2000]). This test resulted in lowering the global-total DMS emission to 18.8 Gg-S yr^{-1}. It also led to decreases

160 in the DMS mixing ratios in the lower troposphere (<5 km) by 59–63% from [MOD_2000], further reducing the model-ATom difference (**Figure S4**). It is noteworthy that the parameterization methods of the sea- and air-side resistance as well as meteorological variabilities, e.g., near-surface air temperature and wind speed, may also contribute to the uncertainties in DMS flux estimation.

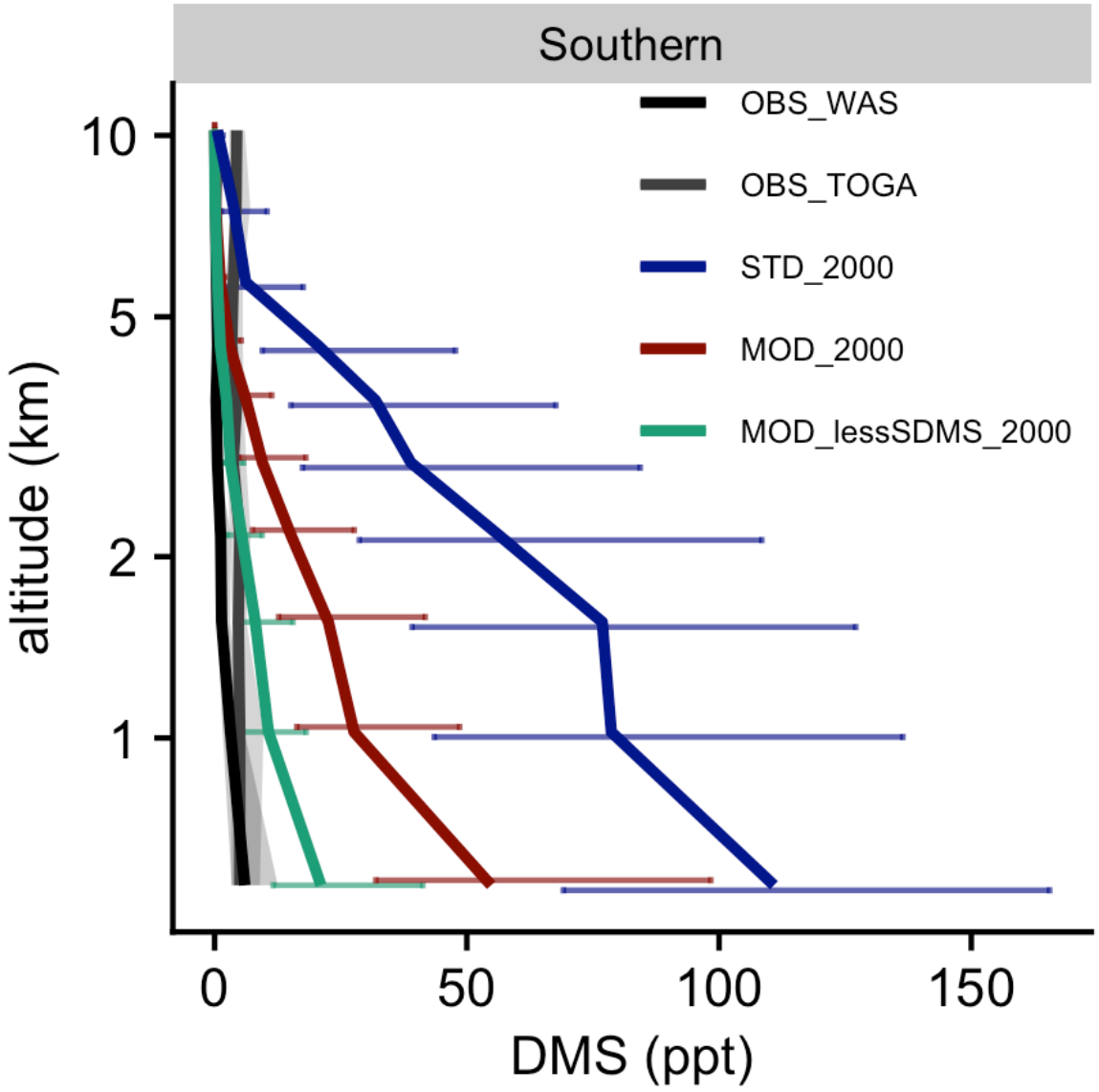

165

Figure S4. DMS vertically binned mean observations from ATom and modeled values. Only the mid-90% of each observational or modeled data set are included in this analysis. Error bars and gray shadings indicate data ranged between corresponding upper and lower quantiles.

4 Global sulfur budgets

Table S1. Global burdens and lifetimes of atmospheric sulfur species in our present-day and preindustrial simulations.

	STD_2000		MOD_2000	
	Burden (Gg-S)	**Lifetime (days)**	**Burden (Gg-S)**	**Lifetime (days)**
DMS	81	1.5	50	0.8
HPMTF	-	-	18	0.9
MSA	-	-	8	0.6
SO_2	370	1.4	365	1.4
[from DMS]	[37]	-	[34]	-
Sulfate	535	4.4	582	4.4
[from DMS]	[126]	-	[178]	-
Others	0.012	-	4.4	-

	STD_1850		MOD_1850	
	Burden (Gg-S)	**Lifetime (days)**	**Burden (Gg-S)**	**Lifetime (days)**
DMS	148	2.6	92	1.5
HPMTF	-	-	36	1.5
MSA	-	-	12	0.6
SO_2	260	2.3	256	2.4
[from DMS]	[57]	-	[50]	-
Sulfate	319	5.6	412	6.2
[from DMS]	[142]	-	[236]	-
Others	0.013	-	8.1	-

5 Sensitivity tests on the production and loss processes of HPMTF

We explore the impact of using a different k_{iso} (isomerization rate of MSP) determined by our recent laboratory experiment and two cloud uptake rates ($k_{HPMTF+cloud}$) on reducing the model-observation deviations. All simulations for the sensitivity tests are performed with our modified chemistry and PD-level emissions, i.e., based on [MOD_2000]. **Table S2** summarizes the model settings and key results of these tests.

Table S2. Summary of the results in the sensitivity tests on the production and loss processes of HPMTF.

k_{iso} (s^{-1}) at 293K	$k_{HPMTF+cloud}$ (s^{-1})	Change* in HPMTF Burden (%)	HPMTF Lifetime (days)	Portion of HPMTF Loss Associated with Cloud Uptake (%)	Change* in Sulfate Burden Relative to DMS-derived Sulfate (%)
0.12	-	+4.1	0.8	-	+4.0
0.12	5×10^{-3}	–85	0.1	68	–8.5
0.12	5×10^{-5}	–52	0.4	28	–7.8
0.04	5×10^{-3}	–86	0.1	69	–6.9
0.04	5×10^{-5}	–52	0.4	28	–7.8

* relative to [MOD_2000]

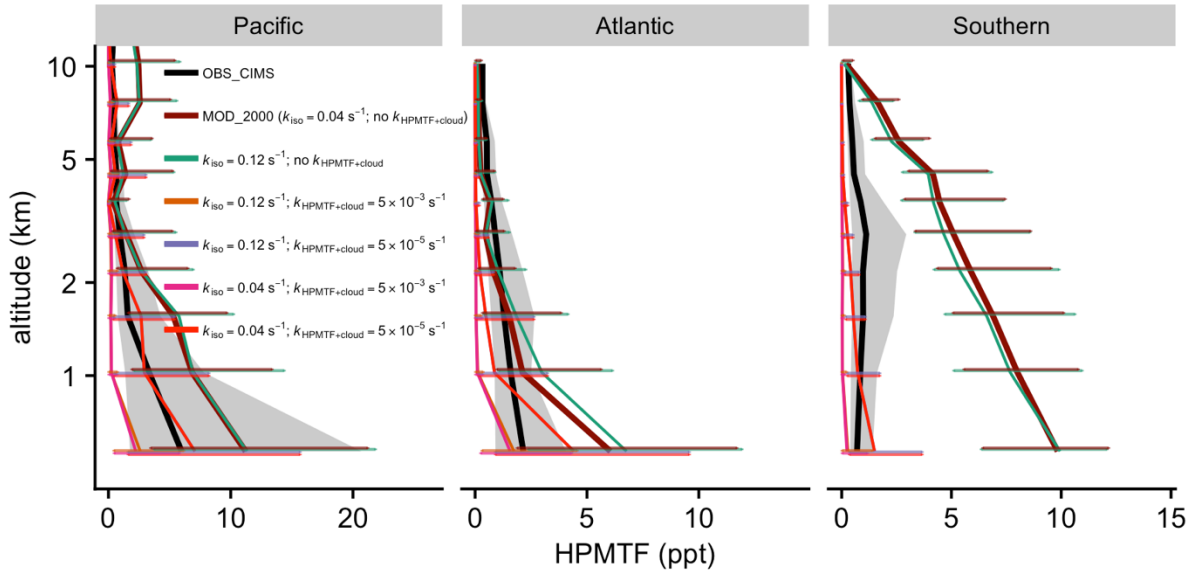

Figure S5. Mean observations and modeled values of HPMTF, vertically binned. Simulations with various settings of the isomerization rates of MSP (k_{iso}) and cloud uptake rate of HPMTF ($k_{HPMTF+cloud}$) are shown. Only the mid-90% of each observational or modeled data set are included in this analysis. Error bars and gray shadings indicate data ranged between corresponding upper and lower quantiles.

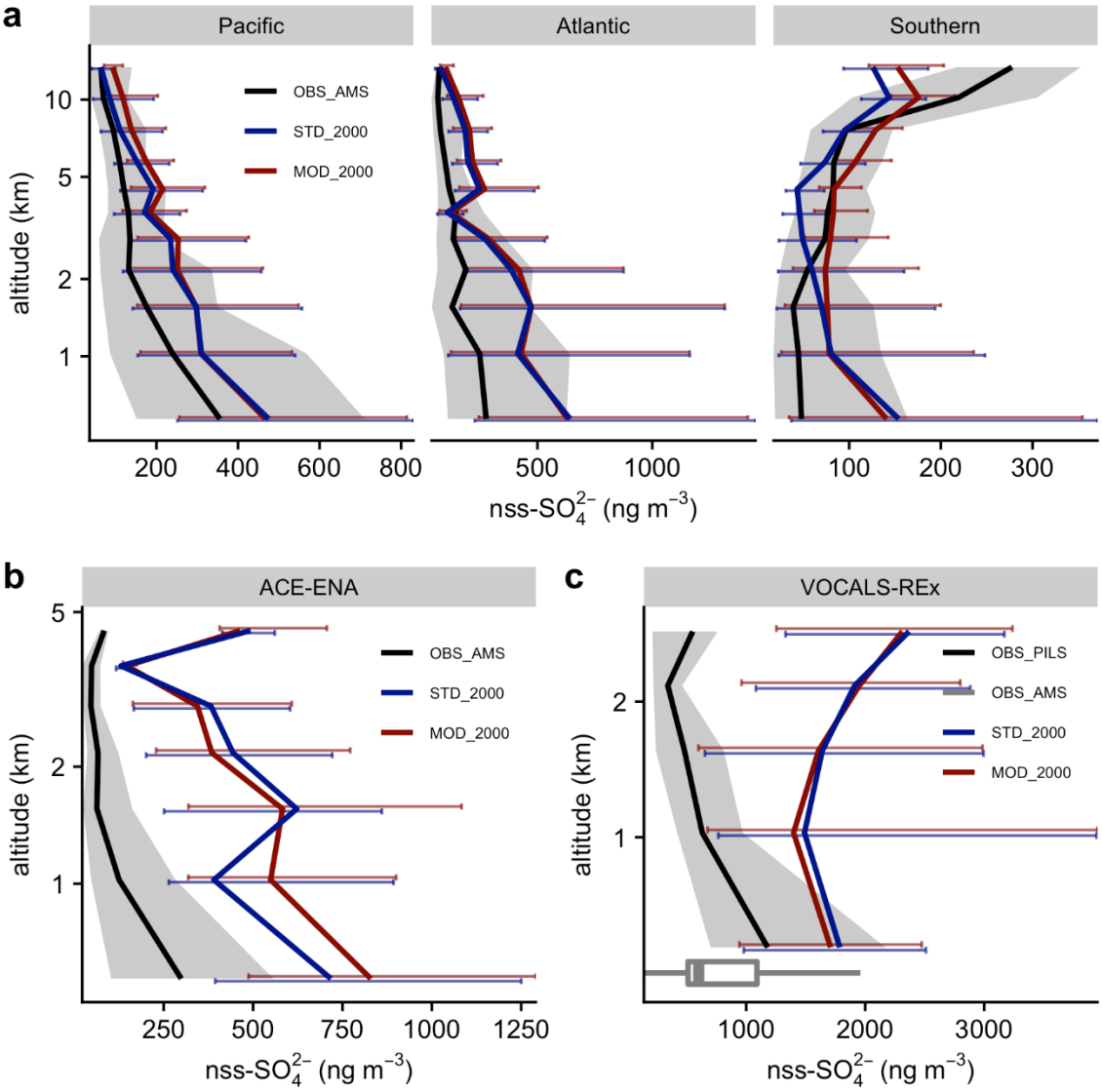

Figure S6. Vertically binned mean sulfate aerosol concentration from our simulations and the observations from: **(a)** ATom; **(b)** ACE-ENA; **(c)** VOCAL-REx. Thick lines show medians. Error bars and gray shadings indicate data ranged between corresponding upper and lower quantiles.

7 Preindustrial spatial distribution of atmospheric sulfur

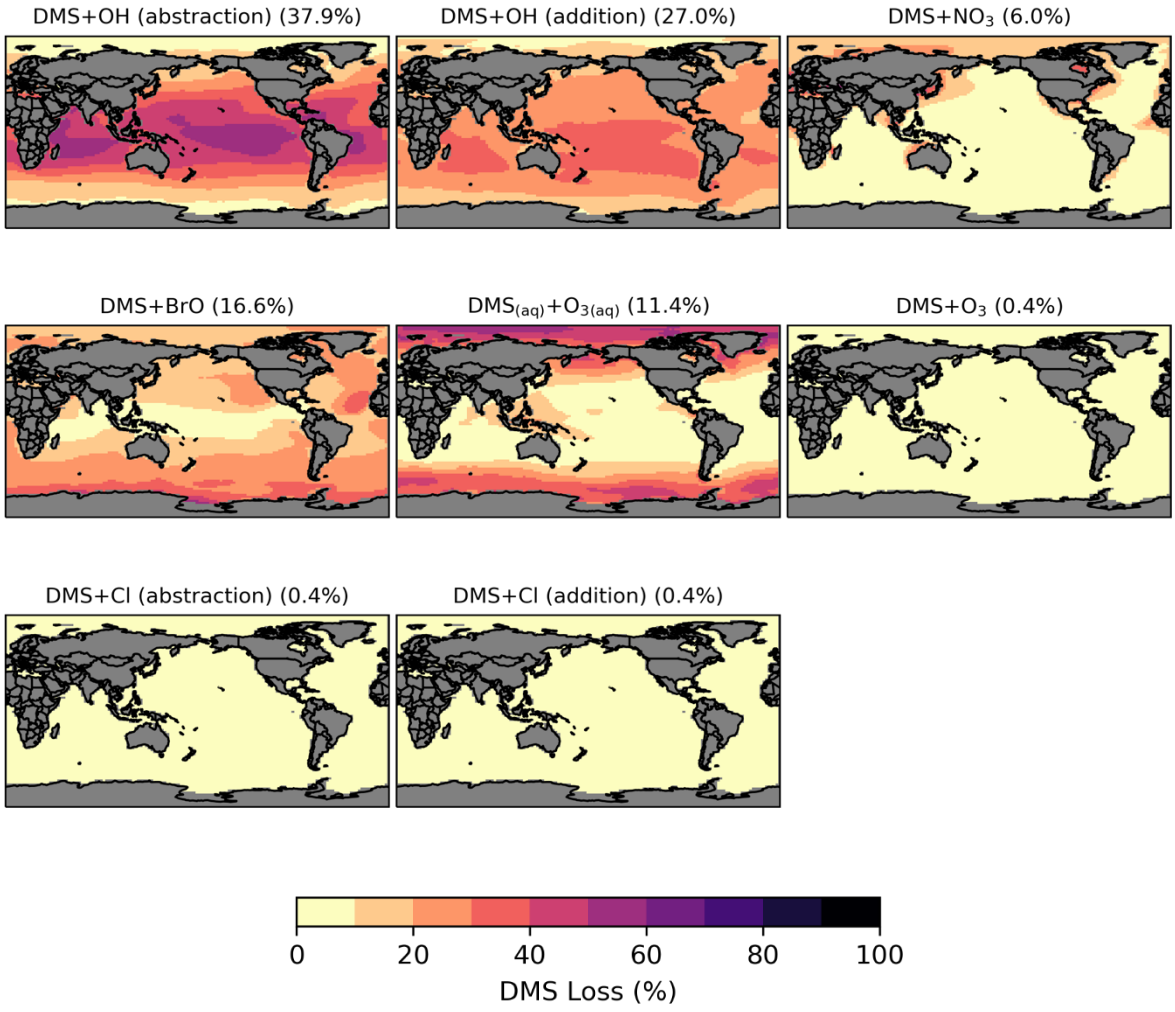

195 **Figure S7.** Global distribution of fractional DMS oxidation (%) from [MOD_1850] through DMS+OH (abstraction), DMS+OH (addition), DMS+NO_3, DMS+BrO, $DMS_{(aq)}+O_{3(aq)}$, DMS+O_3, DMS+Cl (abstraction), and DMS+Cl (addition). Subplots are arranged in the same order of their annual-total oxidation rates as in [MOD_2000] (**Error! Reference source not found.**).

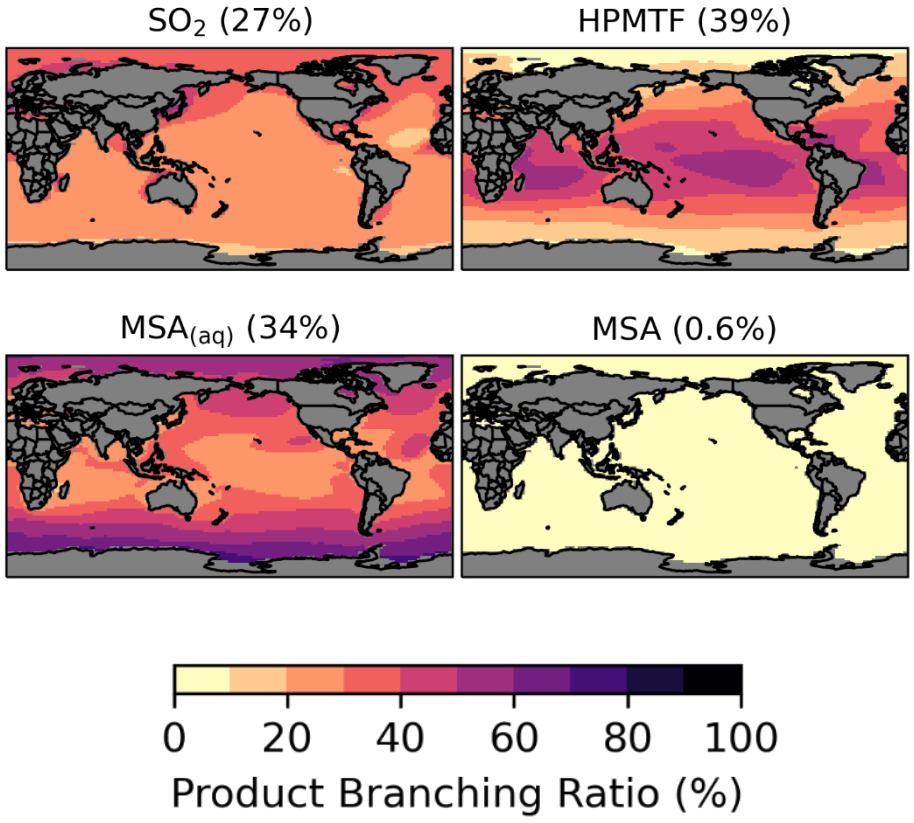

Figure S8. Branching ratio (%) of the multi-phase DMS oxidation pathways in [MOD_1850], considering HPMTF, SO_2, and MSA as terminating products estimated from their annual-total production rates.

8 Spatial distribution of sulfate direct radiative effects

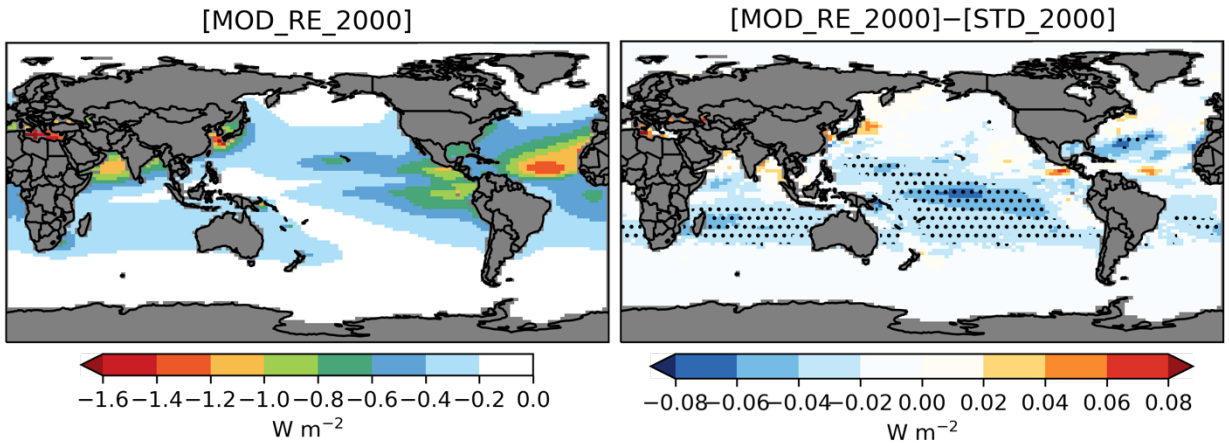

Figure S9. Spatial distribution of annual-mean all-sky sulfate DRE (W m^{-2}) for sulfate aerosol simulated by [MOD_RE_2000] (left), and its difference from the baseline run, i.e. [MOD_2000]–[STD_2000] (right). Dot-overlaying regions indicate statistically significant differences under grid-by-grid two-sample t-tests.

9 Estimation of the direct and indirect radiative forcing of sulfate and MSA

To investigate the joint radiative effect of MSA and sulfate, we discuss in the main text the results of DRE and IRF from simulations with additional chemical reactions that convert MSA aerosol into sulfate. This section explores the impacts of such changes.

Introducing MSA into the model via our DMS chemistry s imposes a substantial impact on radiative balance over the high latitudes. Since the standard CAM6-chem does not include MSA when calculating radiative transfer, we assume that the radiative properties of MSA are identical to sulfate. Then, we perform an extra simulation for each of [MOD_1850] and [MOD_2000] with rapid MSA-to-sulfate conversion to capture the joint radiative effect of MSA and sulfate. We denote them as

[MOD_RE_1850] and [MOD_RE_2000], respectively. This rapid conversion increases the sulfate burden (though lower than the combined burden of sulfate and MSA) but reduces its lifetime. Thus, the results represent a lower bound of the radiative effects and forcing of sulfate and MSA.

The PD MSA and sulfate burdens are 7.5 Gg-S and 582 Gg-S, respectively, from [MOD_2000] while the new sulfate burden is 588 Gg-S in [MOD_RE_2000]. The slightly lower total sulfur aerosol burden is likely due to faster deposition rates of sulfate, but sulfate lifetime maintains at 4.4 days as [MOD_2000]. Similarly, the rapid conversion also induces an increase in PI sulfate burden from 411 Tg-S in [MOD_1850] to 418 Tg-S in [MOD_RE_1850]. Hence, the PD-PI sulfate burden difference of [MOD] is +170 Tg-S (similar to [MOD_RE]) and weaker IRF (+0.76% with respect to [MOD_RE]).

10 Aerosol indirect radiative forcing (IRF)

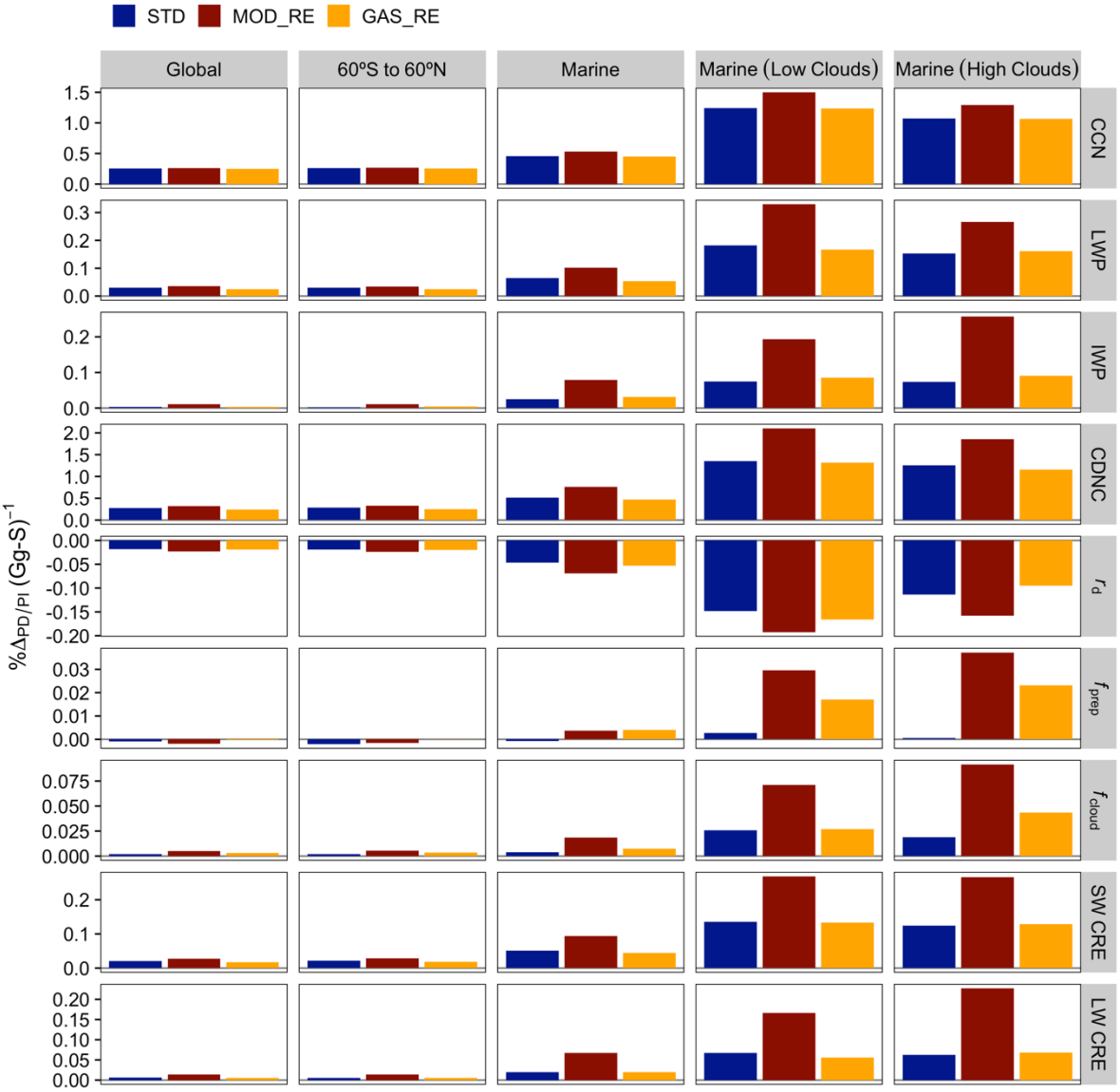

Figure S10. Sensitivity of PI-to-PD percentage changes of cloud condensation nuclei (CCN), liquid water path (LWP), ice water path (IWP), cloud droplet number concentration (CDNC), cloud droplet radius (r_d), frequency of precipitation (f_{prep}), cloud coverage (f_{cloud}), SW CRE, and LW CRE against each unit of increase in sulfate burden, on five spatial scales: global, 60ºS to 60ºN, marine only, marine with low clouds, and marine with high clouds. CCN is estimated using global/regional total value while other variables are global/regional means.

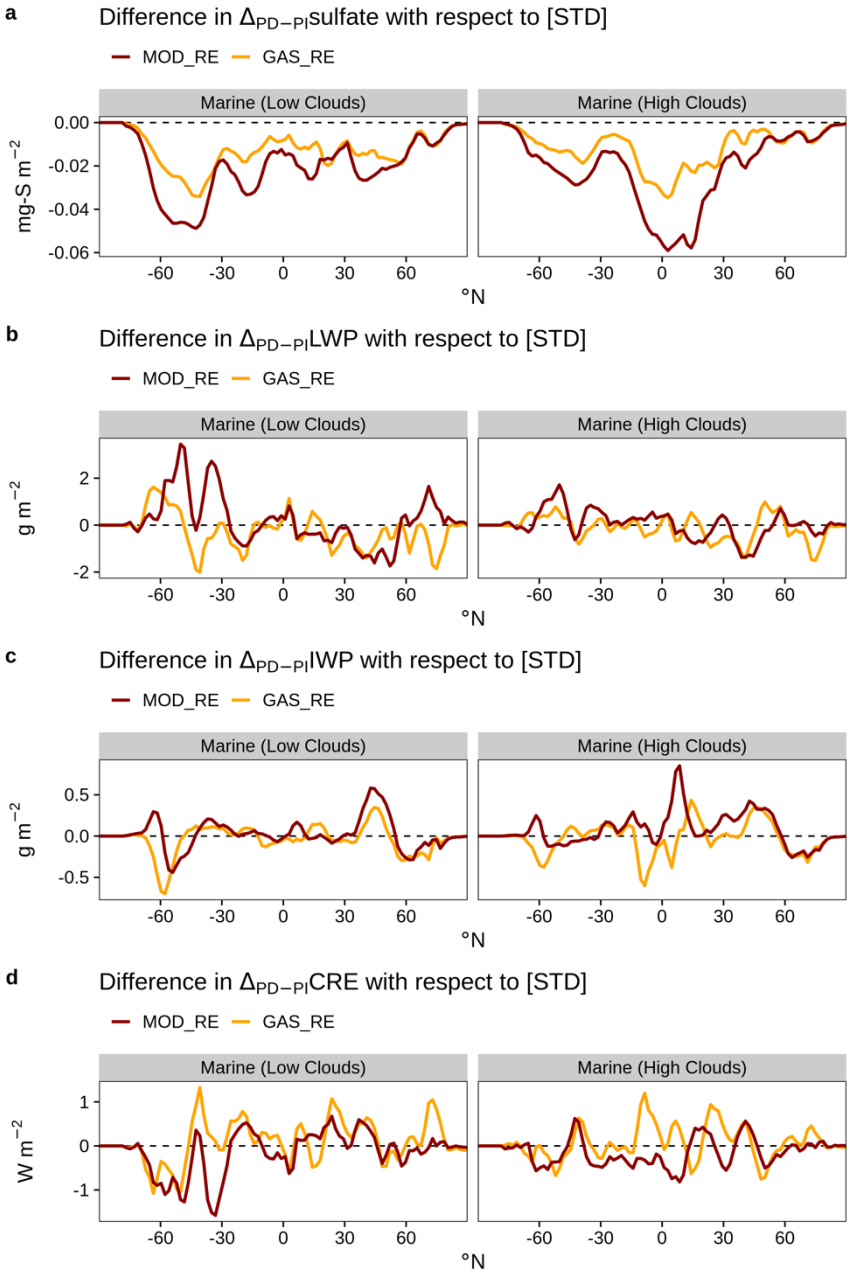
a
Difference in Δ_{PD-PI}sulfate with respect to [STD]
MOD_RE
GAS_RE
Marine (Low Clouds)
Marine (High Clouds)
mg-S m^{-2}
0.00
-0.02
-0.04
-0.06
-60
-30
0
30
60
°N
b
Difference in Δ_{PD-PI}LWP with respect to [STD]
MOD_RE
GAS_RE
Marine (Low Clouds)
Marine (High Clouds)
g m^{-2}
2
0
-2
-60
-30
0
30
60
°N
c
Difference in Δ_{PD-PI}IWP with respect to [STD]
MOD_RE
GAS_RE
Marine (Low Clouds)
Marine (High Clouds)
g m^{-2}
0.5
0.0
-0.5
-60
-30
0
30
60
°N
d
Difference in Δ_{PD-PI}CRE with respect to [STD]
MOD_RE
GAS_RE
Marine (Low Clouds)
Marine (High Clouds)
W m^{-2}
1
0
-1
-60
-30
0
30
60
°N

240

Figure S11. Contrasting the zonal-means of difference in PI-to-PD changes of (a) sulfate column concentration, (b) cloud droplet number concentration (CDNC), (c) liquid water path (LWP), ice water path (IWP), and (d) SW ΔCRE, overlapping with marine low and high clouds, modeled by simulations with different chemistry settings.

245

References

Abdul-Razzak, H. and Ghan, S. J.: A parameterization of aerosol activation: 2. Multiple aerosol types, J. Geophys. Res., 105, 6837–6844, https://doi.org/10.1029/1999JD901161, 2000.

Barth, M. C., Rasch, P. J., Kiehl, J. T., Benkovitz, C. M., and Schwartz, S. E.: Sulfur chemistry in the National Center for Atmospheric Research Community Climate Model: Description, evaluation, features, and sensitivity to aqueous chemistry, J. Geophys. Res., 105, 1387–1415, https://doi.org/10.1029/1999JD900773, 2000.

Binkowski, F. S. and Roselle, S. J.: Models-3 Community Multiscale Air Quality (CMAQ) model aerosol component 1. Model description, J. Geophys. Res., 108, 2001JD001409, https://doi.org/10.1029/2001JD001409, 2003.

Bogenschutz, P. A., Gettelman, A., Morrison, H., Larson, V. E., Schanen, D. P., Meyer, N. R., and Craig, C.: Unified parameterization of the planetary boundary layer and shallow convection with a higher-order turbulence closure in the Community Atmosphere Model: single-column experiments, Geosci. Model Dev., 5, 1407–1423, https://doi.org/10.5194/gmd-5-1407-2012, 2012.

Bogenschutz, P. A., Gettelman, A., Hannay, C., Larson, V. E., Neale, R. B., Craig, C., and Chen, C.-C.: The path to CAM6: coupled simulations with CAM5.4 and CAM5.5, Geosci. Model Dev., 11, 235–255, https://doi.org/10.5194/gmd-11-235-2018, 2018.

Emmons, L. K., Walters, S., Hess, P. G., Guenther, A., Kinnison, D., Laepple, T., Orlando, J., Tie, X., Tyndall, G., Wiedinmyer, C., Baughcum, S. L., and Kloster, S.: Description and evaluation of the Model for Ozone and Related chemical Tracers, version 4 (MOZART-4), Geosci. Model Dev., 25, 2010.

Gettelman, A.: Putting the clouds back in aerosol–cloud interactions, Atmos. Chem. Phys., 15, 12397–12411, https://doi.org/10.5194/acp-15-12397-2015, 2015.

Gettelman, A. and Morrison, H.: Advanced Two-Moment Bulk Microphysics for Global Models. Part I: Off-Line Tests and Comparison with Other Schemes, 28, 1268–1287, https://doi.org/10.1175/JCLI-D-14-00102.1, 2015.

Ghan, S. J.: Technical Note: Estimating aerosol effects on cloud radiative forcing, Atmos. Chem. Phys., 13, 9971–9974, https://doi.org/10.5194/acp-13-9971-2013, 2013.

Ghan, S. J. and Zaveri, R. A.: Parameterization of optical properties for hydrated internally mixed aerosol, J. Geophys. Res., 112, https://doi.org/10.1029/2006JD007927, 2007.

Golaz, J.-C. and Larson, V. E.: A PDF-Based Model for Boundary Layer Clouds. Part I: Method and Model Description, J. Atmos. Sci., 59, 12, 2002.

He, J. and Zhang, Y.: Improvement and further development in CESM/CAM5: gas-phase chemistry and inorganic aerosol treatments, Atmos. Chem. Phys., 14, 9171–9200, https://doi.org/10.5194/acp-14-9171-2014, 2014.

Hess, M., Koepke, P., and Schult, I.: Optical Properties of Aerosols and Clouds: The Software Package OPAC, B. Am. Meteorol. Soc., 79, 831–844, https://doi.org/10.1175/1520-0477(1998)079<0831:OPOAAC>2.0.CO;2, 1998.

Iacono, M. J., Delamere, J. S., Mlawer, E. J., Shephard, M. W., Clough, S. A., and Collins, W. D.: Radiative forcing by long-lived greenhouse gases: Calculations with the AER radiative transfer models, J. Geophys. Res., 113, D13103, https://doi.org/10.1029/2008JD009944, 2008.

Kerminen, V.-M. and Kulmala, M.: Analytical formulae connecting the "real" and the "apparent" nucleation rate and the nuclei number concentration for atmospheric nucleation events, J. Aerosol Sci., 33, 609–622, https://doi.org/10.1016/S0021-8502(01)00194-X, 2002.

Lana, A., Bell, T. G., Simó, R., Vallina, S. M., Ballabrera-Poy, J., Kettle, A. J., Dachs, J., Bopp, L., Saltzman, E. S., Stefels, J., Johnson, J. E., and Liss, P. S.: An updated climatology of surface dimethlysulfide concentrations and emission fluxes in the global ocean, Global Biogeochem. Cycles, 25, https://doi.org/10.1029/2010GB003850, 2011.

Lelieveld, J. and Crutzen, P. J.: Influences of cloud photochemical processes on tropospheric ozone, Nature, 343, 227–233, https://doi.org/10.1038/343227a0, 1990.

Liu, X., Penner, J. E., Ghan, S. J., and Wang, M.: Inclusion of Ice Microphysics in the NCAR Community Atmospheric Model Version 3 (CAM3), J. Clim., 20, 4526–4547, https://doi.org/10.1175/JCLI4264.1, 2007.

Liu, X., Easter, R. C., Ghan, S. J., Zaveri, R., Rasch, P., Shi, X., Lamarque, J.-F., Gettelman, A., Morrison, H., Vitt, F., Conley, A., Park, S., Neale, R., Hannay, C., Ekman, A. M. L., Hess, P., Mahowald, N., Collins, W., Iacono, M. J., Bretherton, C. S., Flanner, M. G., and Mitchell, D.: Toward a minimal representation of aerosols in climate models: description and evaluation in the Community Atmosphere Model CAM5, Geosci. Model Dev., 5, 709–739, https://doi.org/10.5194/gmd-5-709-2012, 2012.

Liu, X., Ma, P.-L., Wang, H., Tilmes, S., Singh, B., Easter, R. C., Ghan, S. J., and Rasch, P. J.: Description and evaluation of a new four-mode version of the Modal Aerosol Module (MAM4) within version 5.3 of the Community Atmosphere Model, Geosci. Model Dev., 9, 505–522, https://doi.org/10.5194/gmd-9-505-2016, 2016.

Merikanto, J., Napari, I., Vehkamäki, H., Anttila, T., and Kulmala, M.: New parameterization of sulfuric acid-ammonia-water ternary nucleation rates at tropospheric conditions, J. Geophys. Res., 112, D15207, https://doi.org/10.1029/2006JD007977, 2007.

Mitchell, D. L., Baran, A. J., Arnott, W. P., and Schmitt, C.: Testing and Comparing the Modified Anomalous Diffraction Approximation, J. Atmos. Sci., 63, 2948–2962, https://doi.org/10.1175/JAS3775.1, 2006.

Morrison, H. and Gettelman, A.: A New Two-Moment Bulk Stratiform Cloud Microphysics Scheme in the Community Atmosphere Model, Version 3 (CAM3). Part I: Description and Numerical Tests, J. Clim., 21, 3642–3659, https://doi.org/10.1175/2008JCLI2105.1, 2008.

Neu, J. L. and Prather, M. J.: Toward a more physical representation of precipitation scavenging in global chemistry models: cloud overlap and ice physics and their impact on tropospheric ozone, Atmos. Chem. Phys., 12, 3289–3310, https://doi.org/10.5194/acp-12-3289-2012, 2012.

Petters, M. D. and Kreidenweis, S. M.: A single parameter representation of hygroscopic growth and cloud condensation nucleus activity, Atmos. Chem. Phys., 11, 2007.

Pincus, R., Barker, H. W., and Morcrette, J.-J.: A fast, flexible, approximate technique for computing radiative transfer in inhomogeneous cloud fields, J. Geophys. Res., 108, https://doi.org/10.1029/2002JD003322, 2003.

Rasch, P. J., Barth, M. C., Kiehl, J. T., Schwartz, S. E., and Benkovitz, C. M.: A description of the global sulfur cycle and its controlling processes in the National Center for Atmospheric Research Community Climate Model, Version 3, J. Geophys. Res., 105, 1367–1385, https://doi.org/10.1029/1999JD900777, 2000.

Seinfeld, J. H., Pandis, S. N., and Noone, K.: Atmospheric chemistry and physics: from air pollution to climate change, 51, 88, 1998.

Vehkamäki, H.: An improved parameterization for sulfuric acid–water nucleation rates for tropospheric and stratospheric conditions, J. Geophys. Res., 107, 4622, https://doi.org/10.1029/2002JD002184, 2002.

Wang, M. and Penner, J. E.: Aerosol indirect forcing in a global model with particle nucleation, Atmos. Chem. Phys., 22, 2009.

Wesely, M. L.: Parameterization of Surface Resistances to Gaseous Dry Deposition in Regional-Scale Numerical Models, 23, 1293–1304, https://doi.org/10.1016/j.atmosenv.2007.10.058, 1989.

Zaveri, R. A., Easter, R. C., Fast, J. D., and Peters, L. K.: Model for Simulating Aerosol Interactions and Chemistry (MOSAIC), J. Geophys. Res., 113, D13204, https://doi.org/10.1029/2007JD008782, 2008.

Zaveri, R. A., Easter, R. C., Singh, B., Wang, H., Lu, Z., Tilmes, S., Emmons, L. K., Vitt, F., Zhang, R., Liu, X., Ghan, S. J., and Rasch, P. J.: Development and Evaluation of Chemistry-Aerosol-Climate Model CAM5-Chem-MAM7-MOSAIC: Global Atmospheric Distribution and Radiative Effects of Nitrate Aerosol, J. Adv. Model Earth Syst., 13, https://doi.org/10.1029/2020MS002346, 2021.